Applied Catalysis B: Environmental 142–143 (2013) 694–704

Contents lists available at SciVerse ScienceDirect

Applied Catalysis B: Environmental

journal homepage: www.elsevier.com/locate/apcatb

Activated carbon as photocatalyst of reactions in aqueous phase

I. Velo-Gala, J.J. López-Peñalver, M. Sánchez-Polo*, J. Rivera-Utrilla

Department of Inorganic Chemistry, Faculty of Science, University of Granada, 18071 Granada, Spain

ARTICLE INFO

Article history:
Received 4 April 2013
Received in revised form 28 May 2013
Accepted 2 June 2013
Available online 11 June 2013

Keywords:
UV radiation
Diatrizoate
Activated carbon
Band gap
Photocatalysis

ABSTRACT

The main objective of this study was to identify the origin of the photocatalytic behavior of activated carbons in the presence of ultraviolet (UV) light. For this purpose, we selected four commercial activated carbons and sixteen gamma radiation-modified carbons derived from these. Sodium diatrizoate was considered as model compound for the degradation study. The results demonstrate that the direct diatrizoate photodegradation rate is influenced by the solution pH. The presence of activated carbon during diatrizoate degradation markedly accelerates its rate of removal, regardless of the activated carbon used. Witco commercial carbon exerts the highest synergic effect in diatrizoate removal by the UV/activated carbon system, with a synergic contribution >53% after the first minute of treatment. The synergic activity of all of the activated carbon samples is enhanced by gamma radiation treatment. The textural properties of the activated carbons show no clear relationship with their synergic contribution. However, the synergic activity of the activated carbon is more greatly enhanced in the samples with higher percentages of surface oxygen, and among these, the samples with higher percentages of ester/anhydride groups and of carbon atoms with sp^2 hybridization. Band gap (E_g) determination of activated carbons revealed that they behave as semiconductor materials and, therefore, as photoactive materials in the presence of UV radiation, given that all E_g values are <4 eV. We also observed that the gamma radiation treatment reduces the band gap values of the activated carbons and that, in a single series of commercial carbons, lower E_g values correspond to higher sodium diatrizoate removal rate values. We highlight that the gamma radiation-modified materials show a higher percentage of carbon atoms with sp^2 hybridization, explaining their superior behavior in the process. Finally, we observed that: (i) the activity of the reutilized activated carbons is similar to that of the original carbons, (ii) the presence of dissolved oxygen enhances the rate of diatrizoate removal by UV/activated carbon, and (iii) the UV radiation treatment produces slight chemical modifications in the activated carbons. Based on these results, an action mechanism for the photocatalytic removal of diatrizoate in the presence of activated carbon is proposed, in which the activated carbon acts as a photocatalyst, promoting electrons of the valence band to the conduction band and increasing the generation of $HO^{\bullet}$ radicals in the medium.

1. Introduction

Numerous pharmaceutical compounds are being studied as part of a group of emerging unregulated pollutants that pose a potential risk for ecosystems and human health [1,2]. These compounds and their degradation byproducts have been found in both surface and ground waters [3–5], because many of them resist removal by conventional urban wastewater treatments. Given the increase in the use and types of these products, there is a clear need for research on measures to avoid their presence in the environment. Iodate contrast media are considered to be model compounds of these pollutants due to their persistence and detection in urban wastewaters, surface waters, and ground waters [5–9].

The iodate contrast media used in hospitals include sodium diatrizoate (DTZ), a highly persistent compound that has been detected in treatment plant effluents, surface waters, and ground waters in ranges from ng L^{-1} to mg L^{-1} [3,5,7,10]. This persistence and its high water solubility mean that DTZ poses a major environmental challenge. DTZ is not mineralized in the environment [11,12] but can be degraded, resulting in stable and potentially more hazardous biodegradation byproducts [12–14]. The resulting concentrations of this contrast medium and its possible metabolites in the environment allow them to accumulate in the food chain,

Abbreviations: AC, activated carbon; AOPs, advanced oxidation processes; E_g, band gap energy; C, activated carbon Ceca; DRS, diffuse reflectance spectra; DTZ, sodium diatrizoate; D_P, mean pore width; HPLC, high performance liquid chromatography; M, activated carbon Merck; pH_{PZC}, pH of point of zero charge; S, activated carbon Sorbo; S_{BET}, surface area determinate by BET; SBW, spectral bandwidth; UV, ultraviolet light; UV/AC, UV/activated carbon system; V_T, total pore volume; W, activated carbon Witco; XFR, X-ray fluorescence; XPS, X-ray photoelectron spectroscopy.

* Corresponding author. Tel.: +34 95824288; fax: +34 958243856.
E-mail address: mansanch@ugr.es (M. Sánchez-Polo).

0926-3373/$ – see front matter © 2013 Elsevier B.V. All rights reserved.
http://dx.doi.org/10.1016/j.apcatb.2013.06.003

with the consequent possible noxious effects on living beings. In this context, Advanced Oxidation Processes (AOPs) appear to be a promising technology for removing organic compounds that are resistant to conventional biological treatments, including DTZ. However, the DTZ degradation rate was only 14% with ozone treatment [15,16] and a maximum of 36% with other AOPs (O_3/UV-low pressure mercury lamp, O_3/H_2O_2) [17]; therefore, DTZ continues to be detected at the end of these treatments. Likewise, another study based on competitive kinetics models for treatment with ozone, Fenton, O_3/H_2O_2, and UV/H_2O_2 obtained similar results in ultrapure water, finding that the highest degradation rates were achieved with UV radiation at 254 nm (96.6%) and photo-Fenton (64.7%) [18].

AOPs include photocatalytic processes, which require the use of luminous radiation capable of producing electronic activation of the catalyst. The energy of this radiation must be in the visible or UV region, and the photocatalyst must be a semiconductive material with an electronic band structure that can generate electron–hole pairs after irradiation at a given wavelength. The electron–hole pairs favor the formation of highly reactive radical species that participate in pollutant degradation. These radicals will derive from reduction or oxidation reactions on whether they are promoted by the electron or hole generated, respectively.

Various materials have been used as photocatalysts, and TiO_2 is one of the most widely applied in water treatments. The considerable research carried out since the publication of the first studies in the 1970s [19] has yielded wide knowledge of the technological possibilities offered by the use of titanium oxides with UV radiation in their elemental polymorphic forms (anatase, rutile, and brookite) and in combination with other materials that act as doping and/or support agents [20–23]. Documented drawbacks of utilizing these materials include: the difficulty of their removal from the treated effluent treated, the need for their recovery and reutilization, the reduced percentage absorption of the solar spectrum, and the high level of recombination of electron–hole pairs. Recent investigations have centered on photocatalysis processes that reduce these disadvantages. The immobilization of these photocatalysts in porous carbon materials is a research line of special interest, as reflected by the exponential increase in the number of publications over the past few years [24–30].

The photocatalytic process can be improved by the physical and chemical properties of activated carbons, especially their large specific surface area, which is usually attributed to the increase in contact surface area between catalyst and pollutant, favored by the action of the carbon as porous support [28,31–33]. However, some carbons play more than a mere support role, as concluded by recent studies [34–36] that obtained 80% mineralization of phenol by photooxidation using UV radiation in the presence of activated carbons and in the absence of semiconductors. These findings are consistent with the capacity of activated carbon to favor photocatalysis in well-known oxidation processes, including ozonation or the use of hydrogen peroxide, in which the carbon itself acts as catalyst [15,16,37] and in which the physical and chemical properties of the carbon influence the ozone decomposition [15,38–40].

With this background, the main aim of this study was to identify the origin of the photocatalytic behavior of activated carbons to remove DTZ in the presence of UV light. For this purpose, we selected four commercial carbons and sixteen gamma-radiated carbons derived from these. The specific objectives were to study: (i) the adsorption kinetics of DTZ on the commercial activated carbons and the gamma-radiated carbons under different experimental conditions; (ii) the DTZ degradation kinetics by direct photolysis with low-pressure UV radiation; (iii) the DTZ photodegradation in the presence of activated carbons; and (iv) the mechanism underlying DTZ degradation with UV light in the presence of activated carbon, determining the role of the physical and chemical properties of the activated carbon in this process.

2. Experimental

2.1. Materials

All chemical products used (sodium diatrizoate, phosphoric acid, and sodium chloride) were high-purity analytical grade and supplied by Sigma–Aldrich. All solutions were prepared with ultrapure water obtained using Milli-Q® equipment (Millipore). The molecular structure of DTZ and its species distribution as a function of solution pH are depicted in Fig. S1 in the Supplementary Materials.

2.2. Determination of DTZ in aqueous solution

DTZ concentrations in solution were determined by high performance liquid chromatography (HPLC) in inverse phase using a chromatograph (Thermo-Fisher) equipped with UV–vis detector and an autosampler with capacity for 120 vials. The chromatographic column was a Nova-Pak® C18 (4 μm particle size; 3.9 × 150 mm). The mobile phase was 80% of water solution (1% phosphoric acid) and 20% ultrapure water, in isocratic mode, with 2.0 mL min^{-1} flow; the detector wavelength was set at 254 nm and injection volume was 100 μL.

2.3. Analysis of DTZ UV–vis absorption spectrum

The DTZ absorption spectrum was determined by using a spectrophotometer (Genesys 5), running a wavelength scan for a DTZ concentration of 25 mg L^{-1} at pH values of 2, 6, 9, and 12.

2.4. Gamma radiation treatment of activated carbons

We used commercial activated carbons Sorbo (S), Merck (M), Ceca (C), and Witco (W) in their original form and after gamma radiation treatment.

Activated carbons were treated using a model 30J MARK-I gamma irradiator (Shepherd & Associates) at the Experimental Radiology Unit of the Granada University Scientific Instrumentation Center (Spain). The equipment includes four sources of ^{137}Cs with a total combined activity of 3.70×10^{13} Bq (1000 Ci). It has three irradiation positions for different dose rates: position 1 (3.83 Gy min^{-1}); position 2 (1.66 Gy min^{-1}); and position 3 (1.06 Gy min^{-1}). In the present study, carbons were irradiated in position 1, receiving a total dose of 25 kGy.

The four activated carbons were irradiated by introducing 5.0 g of each in 50 mL plastic tubes and adding ultrapure water to fill the tubes. Before their irradiation, samples were bubbled with nitrogen to avoid the presence of dissolved oxygen, and the tubes were sealed to avoid air entry. These irradiated samples were designated C-0, M-0, S-0, and W-0, respectively. The predominant radiolytic species in the medium were modified by irradiating the samples in the presence of: (i) 1000 mg L^{-1} Cl^- and pH = 1.0, because the chloride ion acts as scavenger of $OH^•$ and $e_{aq}{}^-$ radicals [41] (Reactions 1–8) and Reaction 9 takes place at this pH [42], producing a majority concentration of $H^•$ in the medium (samples C—$H^•$, M—$H^•$, S—$H^•$, and W—$H^•$, were obtained under these conditions); (ii) 1000 mg L^{-1} Br^- and pH = 7.5, because the bromide ion acts as scavenger of the $HO^•$ radical, giving rise to Reactions 10–13 [43–45], and this medium pH favors Reaction 14 [42], so that the majority species in the medium is $e_{aq}{}^-$ (samples C—$e^-{}_{aq}$, M—$e^-{}_{aq}$, S—$e^-{}_{aq}$, and W—$e^-{}_{aq}$); and (iii) 1000 mg L^{-1} $NO_3{}^-$ and pH = 12.5, because Reactions 14–16 take place under these conditions [37,42,45] and anion nitrate acts as $H^•$ and $e_{aq}{}^-$ scavenger, so that the majority

species in the medium is the $HO^{\bullet}$ radical (samples C—$HO^{\bullet}$, M—$HO^{\bullet}$, S—$HO^{\bullet}$, and W—$HO^{\bullet}$).

$$Cl^- + HO^{\bullet} \rightarrow HClO^{\bullet -}, \quad k = 4.3 \times 10^9\ M^{-1}\ s^{-1} \tag{1}$$

$$HClO^{\bullet -} \rightarrow Cl^- + HO^{\bullet}, \quad k = 6.1 \times 10^9\ M^{-1}\ s^{-1} \tag{2}$$

$$HClO^{\bullet -} + e_{aq}{}^- \rightarrow Cl^- + OH^-, \quad k = 1.0 \times 10^{10}\ M^{-1}\ s^{-1} \tag{3}$$

$$HClO^{\bullet -} + H_3O^+ \rightarrow Cl^{\bullet} + 2H_2O, \quad k = 2.0 \times 10^{10}\ M^{-1}\ s^{-1} \tag{4}$$

$$Cl^{\bullet} + H^{\bullet} \rightarrow Cl^- + H^+, \quad k = 1.0 \times 10^{10}\ M^{-1}\ s^{-1} \tag{5}$$

$$Cl^{\bullet} + Cl^- \rightarrow Cl_2{}^{\bullet -}, \quad k = 2.0 \times 10^{10}\ M^{-1}\ s^{-1} \tag{6}$$

$$Cl_2{}^{\bullet -} + e_{aq}{}^- \rightarrow 2Cl^-, \quad k = 1.0 \times 10^{10}\ M^{-1}\ s^{-1} \tag{7}$$

$$Cl_2{}^{\bullet -} + H^{\bullet} \rightarrow 2Cl^- + H^+, \quad k = 8.0 \times 10^9\ M^{-1}\ s^{-1} \tag{8}$$

$$H_3O^+ + e_{aq}{}^- \rightarrow H^{\bullet} + H_2O, \quad k = 2.2 \times 10^{10}\ M^{-1}\ s^{-1} \tag{9}$$

$$Br^- + HO^{\bullet} \rightarrow HBrO^{\bullet -}, \quad k = 1.1 \times 10^{10}\ M^{-1}\ s^{-1} \tag{10}$$

$$HBrO^{\bullet -} \rightarrow Br^{\bullet} + OH^-, \quad k = 4.2 \times 10^6\ M^{-1}\ s^{-1} \tag{11}$$

$$Br^{\bullet} + Br^- \rightarrow Br_2{}^{\bullet -}, \quad k = 1.0 \times 10^{10}\ M^{-1}\ s^{-1} \tag{12}$$

$$Br_2{}^{\bullet -} + Br_2{}^{\bullet -} \rightarrow Br_3{}^{\bullet -} + Br^-, \quad k = 3.4 \times 10^9\ M^{-1}\ s^{-1} \tag{13}$$

$$H^{\bullet} + OH^- \rightarrow e_{aq}{}^- + H_2O, \quad k = 2.0 \times 10^7\ M^{-1}\ s^{-1} \tag{14}$$

$$e_{aq}{}^- + NO_3{}^- \rightarrow NO_3{}^{\bullet 2-}, \quad k = 9.7 \times 10^9\ M^{-1}\ s^{-1} \tag{15}$$

$$H^{\bullet} + NO_3{}^- \rightarrow NO_2{}^{\bullet} + HO^-, \quad k = 4.4 \times 10^6\ M^{-1}\ s^{-1} \tag{16}$$

The carbons were designated according to the radical present under gamma irradiation conditions (see Table 1).

The particle size of all carbon samples used was <0.25 mm. All activated carbon samples were stored in a sealed container in an oven at 383 K before use.

2.5. Chemical and textural characterization of the activated carbons

All activated carbon samples were texturally (N_2 adsorption at 77 K, CO_2 adsorption at 273 K) and chemically (elemental analysis, mineral material percentage, X-ray fluorescence (XRF), and X-ray photoelectron spectroscopy (XPS)) characterized. Our research group previously reported the techniques used for the chemical and textural characterization of the samples [16,39,46]. The pH of point of zero charge (pH_{pzc}) of the activated carbons was determined by preparing 25 mL solutions of 0.01 N NaCl at different initial pH values obtained by adding different volumes of NaOH (0.01 N) or HCl (0.01 N). Nitrogen was bubbled through the solutions to avoid CO_2 dissolution, and 50 mg activated carbon was subsequently added. The activated carbon and solutions were maintained in contact for 48 h, and the final solution pH was then determined. The initial pH was plotted against the final pH, and the pH at the cut-off point of the curve obtained with the straight line corresponding to initial pH = final pH was considered the pH_{pzc}. The main physical and chemical characteristics of the carbons are shown in Tables 1S–4S in supporting information. Briefly, the results presented in Tables 1S–4S show that gamma radiation can modify activated carbon chemical properties without modifying their textural characteristics. Thus, gamma treatment increases superficial oxygen content and carbon atoms with sp^2 hybridation. In addition, the textural and chemical properties of the treated material depends both of the treatment used and the raw material.

2.6. Photolysis of sodium diatrizoate

DTZ degradation experiments using UV radiation and UV/activated carbon (UV/AC) were conducted in a photoreactor (inner diameter of 13 cm × height of 45 cm) with walls of stainless steel. The photoreactor is equipped with a sample holder with a capacity for 6 quartz tubes (wall-width of 3 mm, inner diameter of 15 mm, height of 300-mm) that have a 92% transmittance for a wavelength of 254 nm. A low-pressure mercury lamp (Hg 253.70 nm) Heraeus Noblelight, model TNN 15/32 (15 W), is placed in the center of the sample holder to ensure uniform irradiation of the six quartz tubes. The photoreactor was filled with ultrapure water that surrounded the sample holder and mercury lamp and was maintained in continuous recirculation at a constant temperature (298.0 ± 0.2 K) using a Frigiterm ultrathermostat. The photoreactor was equipped with a magnetic agitation system for maintaining the solutions within the quartz tubes under constant agitation.

For the study of direct DTZ photolysis, three 25 mg L^{-1} DTZ solutions were prepared at pH 2, 6.5, and 12, and 30 mL of the respective solutions were placed in the quartz tubes in the photoreactor. These solutions were maintained under constant agitation during the entire experiment at a temperature of 298 K and with the application of UV light at 253.70 nm wavelength. Samples were drawn from each solution at regular time intervals for subsequent measurement of the DTZ concentration.

2.7. Diatrizoate degradation by the UV/activated carbon system

Experimental data for DTZ photodegradation in the presence of activated carbon were obtained by the UV irradiation (253.70 nm) of 25 mg L^{-1} solutions of DTZ in the presence of 5 mg activated carbon at pH 6.5 and 298 K under constant agitation. As in Section 2.6, samples were drawn at regular time intervals to follow DTZ degradation kinetics. Samples were immediately filtered by Millipore disk filters (0.45 μm) to remove the activated carbon.

2.8. Diatrizoate adsorption kinetics on activated carbons

Experimental data for DTZ adsorption kinetics on activated carbons were obtained by placing 5 mg of activated carbon in contact with 30 mL of 25 mg L^{-1} DTZ solution at 298 K and pH 6.5. Samples were drawn at regular time intervals to determine the DTZ concentration for calculation of the amount adsorbed. The experimentation conditions for the adsorption process were the same as for UV degradation in the presence of activated carbon.

2.9. Diatrizoate photodegradation in the presence of saturated activated carbons

In order to determine whether the activated carbon truly maintains its photoactive properties, we studied the maintenance of its capacity to enhance the effect of DTZ photolysis over time. For this purpose, we prepared a solution of 100 mg L^{-1} DTZ at pH 6.5 to ensure the presence of the compound throughout the experiment, allowing its concentration to be followed throughout the process. We placed 30 mL of this solution in the quartz tube of the photoreactor and added 20 mg of activated carbon, maintaining this suspension under UV irradiation (253.70 nm) for 15 min. Carbons S-0 and W-$e^-{}_{aq}$ were selected as representative carbons. After the treatment, the carbons were dried in an oven at 50 °C and were then reutilized under the same experimental conditions as in Section 2.7.

Table 1
Nomenclature of the activated carbon samples used.

Ceca series	C	Original Ceca carbon
	C—H$^{\bullet}$	Ceca carbon irradiated in the presence of H$^{\bullet}$ radical
	C—e^-_{aq}	Ceca carbon irradiated in the presence of e^-_{aq}
	C—HO$^{\bullet}$	Ceca carbon irradiated in the presence of HO$^{\bullet}$ radical
	C-0	Ceca carbon irradiated in the presence of all radicals
Merck series	M	Original Merck carbon
	M—H$^{\bullet}$	Merck carbon irradiated in the presence of H$^{\bullet}$ radical
	M—e^-_{aq}	Merck carbon irradiated in the presence of e^-_{aq}
	M—HO$^{\bullet}$	Merck carbon irradiated in the presence of HO$^{\bullet}$ radical
	M-0	Merck carbon irradiated in the presence of all radicals
Sorbo series	S	Original Sorbo carbon
	S—H$^{\bullet}$	Sorbo carbon irradiated in the presence of H$^{\bullet}$ radical
	S—e^-_{aq}	Sorbo carbon irradiated in the presence of e^-_{aq}
	S—HO$^{\bullet}$	Sorbo carbon irradiated in the presence of HO$^{\bullet}$ radical
	S-0	Sorbo carbon irradiated in the presence of all radicals
Witco series	W	Original Witco carbon
	W—H$^{\bullet}$	Witco carbon irradiated in the presence of H$^{\bullet}$ radical
	W—e^-_{aq}	Witco carbon irradiated in the presence of e^-_{aq}
	W—HO$^{\bullet}$	Witco carbon irradiated in the presence of HO$^{\bullet}$ radical
	W-0	Witco carbon irradiated in the presence of all radicals

2.10. Diffuse reflectance spectra

Diffuse reflectance spectra (DRS) of the powdered carbons were obtained by using a VARIAN CARY-5E double-beam UV–vis and near infrared absorption spectrophotometer with wavelength measurements from 200 nm (6.20 eV) through 2000 nm (0.62 eV); the data were acquired at 1-nm intervals using a spectral bandwidth (SBW) of 2 nm for the whole spectrum with the exception of the infrared region, in which the SBW is not fixed. The Grating Switching Wavelength and Detector Switching Wavelength were 800 nm, and the Source Switching Wavelength was 310 nm. Baseline spectra were obtained from a sample of pressed barium sulfate powder. Samples were prepared by grinding 10 mg carbon with 100 mg barium sulfate.

3. Results and discussion

3.1. Diatrizoate degradation by direct photolysis with UV radiation

The effectiveness of UV radiation in DTZ removal from waters was analyzed by obtaining DTZ (25 mg L^{-1}) photodegradation kinetics as a function of the pH. Table 2 exhibits the kinetic constants obtained. The reaction rate constants (k_{OB}) for the three DTZ ionization states (Fig. 1S in the Supplementary Materials) are very similar, indicating that DTZ photodegradation is not influenced by the solution pH.

Table 2
Experimental results of DTZ degradation by direct photolysis.

Exp. num.	pH	k_{OB} (min^{-1})	Φ_λ (mol $Einstein^{-1}$)	% Degradation (15 min)
1	2	0.15 ± 0.50	0.023 ± 0.005	98.7 ± 0.5
2	6.5	0.17 ± 0.40	0.026 ± 0.004	98.5 ± 0.4
3	12	0.14 ± 0.50	0.022 ± 0.005	97.8 ± 0.5

Based on the degradation rate constants obtained (by a first-order kinetic model) at the different pH values, we determined the quantum yield, i.e., the moles of compound per photon absorbed by the system. The following equation was used to calculate the quantum yield of the different chemical species of DTZ:

$$K_\lambda = 2.303 \times E_\lambda \times \varepsilon_\lambda \times \Phi_\lambda \quad (1)$$

where Φ_λ (mol $Einstein^{-1}$) is the quantum yield, K_λ (s^{-1}) is the DTZ photodegradation rate constant, $E_\lambda = 6.16 \times 10^{-3}$ (Einstein s^{-1} m^{-2}) is the radiant energy emitted by the lamp at the wavelength of 253.70 nm, and ε_λ (m^2 mol^{-1}) is the molar absorption coefficient of the compound at the given wavelength.

Table 2 lists the quantum yields determined at the different pH values, confirming that the DTZ photodegradation yield is independent of the medium pH. In order to explain these results, we determined the DTZ absorption spectrum and the emission spectrum of the lamp (Fig. 1). Both spectra reveal the effectiveness of UV radiation to remove DTZ from the medium; the absorption spectrum shows that the UV radiation emitted by the lamp is highly

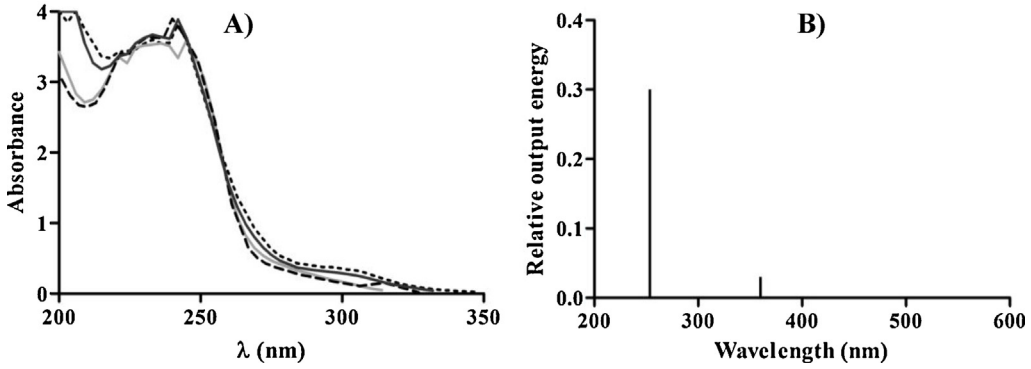

Fig. 1. (A) DTZ adsorption spectrum at different pH values (___ pH = 2; - - pH = 6; ––pH = 9; . . . .pH = 12) and (B) emission spectrum of the low-pressure lamp used.

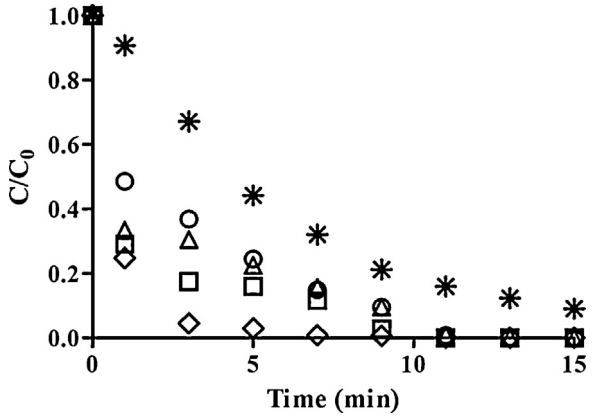

Fig. 2. DTZ degradation by direct photolysis (*) and by the UV/AC system with activated carbons C (◯), M (△), S (□), or W (◊). $[DTZ]_0 = 25\ mg\ L^{-1}$; pH = 6.5; $T = 298\ K$.

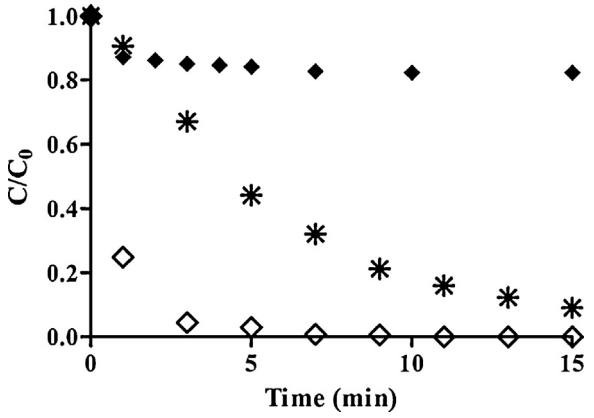

Fig. 3. DTZ degradation by the UV/AC system. Direct photolysis (*), adsorption on activated carbon W (♦), UV/W (◊). $[DTZ]_0 = 25\ mg\ L^{-1}$; pH = 6.5; $T = 298\ K$.

absorbed by the compound, regardless of the ionization state of DTZ.

3.2. Diatrizoate degradation with UV light in the presence of activated carbon

After studying DTZ direct photolysis by UV radiation, we investigated the degradation of this compound when activated carbon was present during the photolytic process (UV/AC). Fig. 2 depicts DTZ removal by UV radiation and by the simultaneous use of UV radiation and activated carbons C, S, M, or W. It is observed that the removal rate is markedly increased by the presence of activated carbon.

Based on the degradation kinetics obtained, we calculated the values of the reaction rate constants in Table 3. The values of these constants confirm the increase in reaction rate observed in the degradation kinetics. This may be attributable to the contribution to the overall removal process of DTZ adsorption on the activated carbons. For this reason, we obtained the DTZ adsorption kinetics on all of the activated carbon samples. Fig. 3 shows, as an example, the results obtained for carbon W. We can observe that there is virtually no DTZ adsorption on W, although this is the activated carbon that produced the greatest increase in DTZ removal by the UV/AC system (Fig. 3). These results indicate that DTZ adsorption on activated carbon is not the sole cause for the increase in DTZ removal in the UV/AC system and that the activated carbon must make other types of contribution to the overall removal process.

The role of activated carbon in DTZ removal process by UV/AC was further explored by determining the percentage removal (designated "synergic effect") of the carbons, which was calculated by subtracting the adsorptive and photolytic contributions from the global removal percentage in the UV/AC system (Eq. (18)). Results are listed in Table 3.

$$\%S_{UV/CA} = \%D_{UV/CA} - \%D_{UV} - \%A_{CA} \quad (18)$$

where $\%S_{UV/CA}$ is the percentage DTZ removal due to the synergic effect produced by the presence of activated carbon during exposure to UV radiation, $\%D_{UV/CA}$ is the total percentage DTZ removal in the photocatalytic process UV/AC, $\%D_{UV}$ is the percentage DTZ degradation by direct photolysis, and $\%A_{CA}$ is the percentage DTZ removal by adsorption on the activated carbon.

Among the different commercial activated carbons used, the results in Table 3 show that carbon *S* made the highest adsorptive contribution to the global removal process and carbon W the lowest. However, we highlight that carbon W exerts the greatest synergic effect on DTZ removal by the UV/AC system, with a synergic contribution of >53% after the first minute of treatment.

Fig. 4 depicts the time course of the synergic contribution to the overall DTZ removal by the UV/AC system for the four original activated carbons. The results obtained indicate that, regardless of

Table 3
Removal fractions and reaction rate constants for DTZ removal by UV/AC. $[DTZ]_0 = 25\ mg\ L^{-1}$; pH = 6.5; $T = 298\ K$.

Exp. num.	Activated carbon	k_{OB} (15 min) (min^{-1})	% UV degradation (1 min)	% Removal by adsorption (1 min)	% Removal by UV/AC (1 min)	% Synergic removal (1 min)
4	C	0.47 ± 0.01	9.29	14.20	51.50	28.01
5	C—$H^{\bullet}$	0.75 ± 0.04	9.29	11.70	49.79	28.80
6	C—e_{aq}^-	0.69 ± 0.03	9.29	11.60	44.61	23.72
7	C—$HO^{\bullet}$	1.05 ± 0.05	9.29	17.00	53.99	27.70
8	C-0	2.05 ± 0.00	9.29	12.90	87.09	64.90
9	M	0.53 ± 0.04	9.29	18.70	66.60	38.61
10	M—$H^{\bullet}$	1.06 ± 0.02	9.29	30.40	65.38	25.69
11	M—e_{aq}^-	1.05 ± 0.04	9.29	0.86	65.04	54.89
12	M—$HO^{\bullet}$	0.93 ± 0.05	9.29	17.00	62.36	36.07
13	M-0	0.69 ± 0.04	9.29	12.40	53.05	31.36
14	S	0.59 ± 0.03	9.29	28.80	71.00	32.91
15	S—$H^{\bullet}$	0.42 ± 0.05	9.29	8.49	45.00	27.22
16	S—e_{aq}^-	0.28 ± 0.02	9.29	9.07	32.49	14.13
17	S—$HO^{\bullet}$	1.03 ± 0.04	9.29	14.80	64.10	39.91
18	S-0	1.07 ± 0.02	9.29	7.67	47.00	30.04
19	W	1.42 ± 0.04	9.29	12.80	75.20	53.11
20	W—$H^{\bullet}$	1.02 ± 0.04	9.29	1.04	69.47	59.14
21	W—e_{aq}^-	5.06 ± 0.06	9.29	1.02	100	89.69
22	W—$HO^{\bullet}$	5.26 ± 0.06	9.29	1.67	92.81	81.85
23	W-0	0.99 ± 0.01	9.29	8.23	62.87	45.35

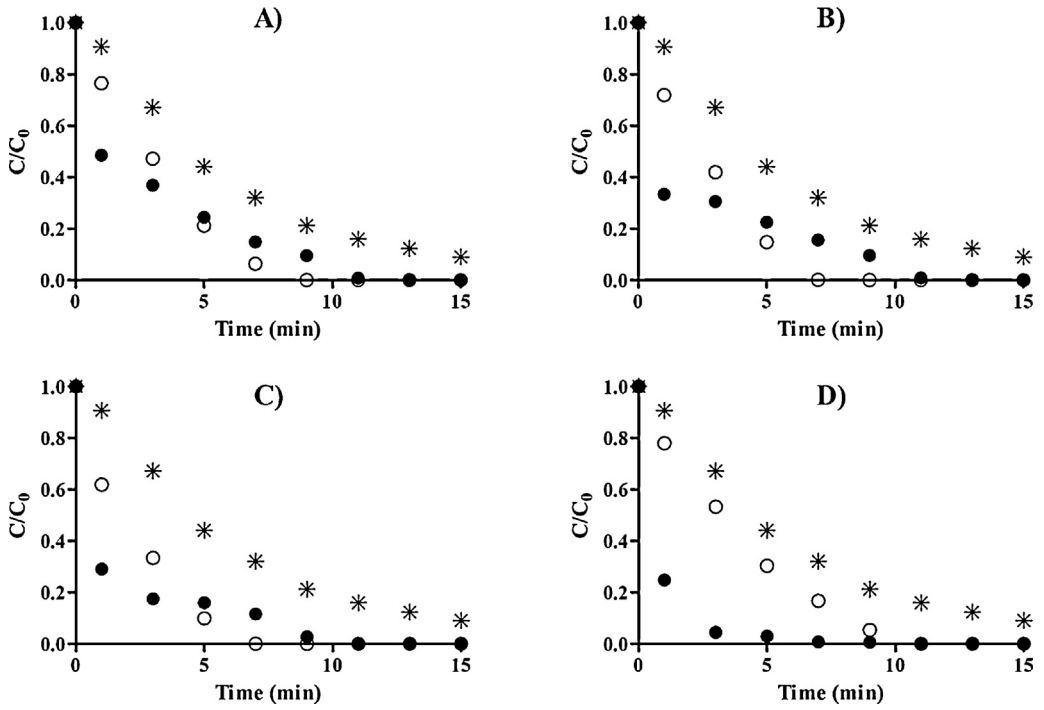

Fig. 4. DTZ removal by the UV/AC system. (*), Direct photolysis; (●), UV/AC; (○), UV + adsorption. (A) Carbon C; (B) Carbon M; (C) Carbon S; (D) Carbon W. $[DTZ]_0 = 25\ mg\ L^{-1}$; pH = 6.5; $T = 298\ K$.

the activated carbon used, the synergic contribution decreases with longer treatment time. This may be attributable to: (i) adsorption of DTZ and degradation compounds on the activated carbon surface that hinders the access of UV radiation to its active sites, and/or (ii) modifications by UV radiation of the chemical functionalities on the surface of the activated carbon, reducing its synergic activity.

In order to explain the results in Fig. 4, we conducted DTZ degradation experiments with the UV/AC system using DTZ-saturated activated carbons. Fig. 5 shows, as an example, the results obtained for carbon S (carbon with higher adsorptive contribution to the global removal process). There is a decrease in the reaction rate at the beginning of the UV/saturated AC process due to the absence of DTZ removal by adsorption; however, the percentage degradation values continue to be higher than those obtained by direct photolysis, confirming that DTZ adsorption is not the most important effect in the reduction of the synergic activity of the activated carbon.

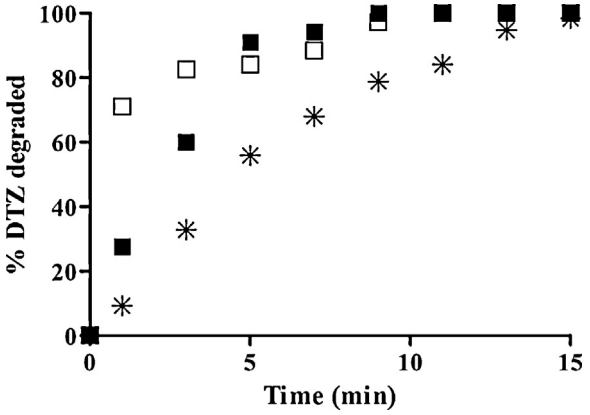

Fig. 5. DTZ degradation by the UV/AC system using saturated activated carbon. (*), Direct photolysis; (□), UV/carbon S; (■), UV/saturated carbon S. $[DTZ]_0 = 25\ mg\ L^{-1}$; pH = 6.5; $T = 298\ K$.

The results in Fig. 4 and Table 3 show no clear relationship with the chemical and textural characteristics of the four activated carbons (Tables 1S–4s, in supporting information). It is interesting to note that the results obtained using TiO_2 as photocatalyst of DTZ photodegradation process show that only a 12.6% of initial concentration of DTZ was degraded after 1 min of treatment with a $k_{ob} = 0.138 \pm 0.002\ min^{-1}$. Thus, the results presented in Table 3 indicate that the synergetic effect of activated carbons is higher than the value obtained for UV/TiO_2.

3.3. Influence of the surface chemistry of activated carbon on diatrizoate degradation by the UV/AC system

We studied DTZ photodegradation in the presence of carbons that had undergone different gamma irradiation treatments. The treatments modified the surface chemistry of the carbons (Tables 2S and 4S, in supporting information) but not their textural characteristics (Table 1S, in supporting information). Thus, we obtained carbons treated with reducing agents (solvated electrons, e^-_{aq}, and hydrogen atoms, $H^\bullet$) and carbons treated with oxidizing agents ($HO^\bullet$ radicals). The nomenclature of the resulting carbons and their chemical and textural characteristics are given in Table 1 and Tables 1S–4S, in supporting information.

Fig. 6 depicts the time course of the relative DTZ concentration during UV/AC treatment of the four series of activated carbons. Table 3 exhibits the kinetic constants obtained and the synergic contribution to the global DTZ removal process.

We shall first discuss the results of carbon W (Fig. 6D), the activated carbon showing the greatest synergic activity. According to the results, the carbons producing the greatest increase in DTZ removal are W-e^-_{aq} and W—$HO^\bullet$, whereas no substantial increase after 1 min of treatment in DTZ removal is observed using the sample treated with hydrogen atoms (W—$H^\bullet$). In addition, Table 3 shows that the synergic contribution of samples W—e^-_{aq} and W—$HO^\bullet$ to the overall removal process for one minute of treatment is markedly higher than the contribution of the original carbon (W). These results appear to indicate that, regardless

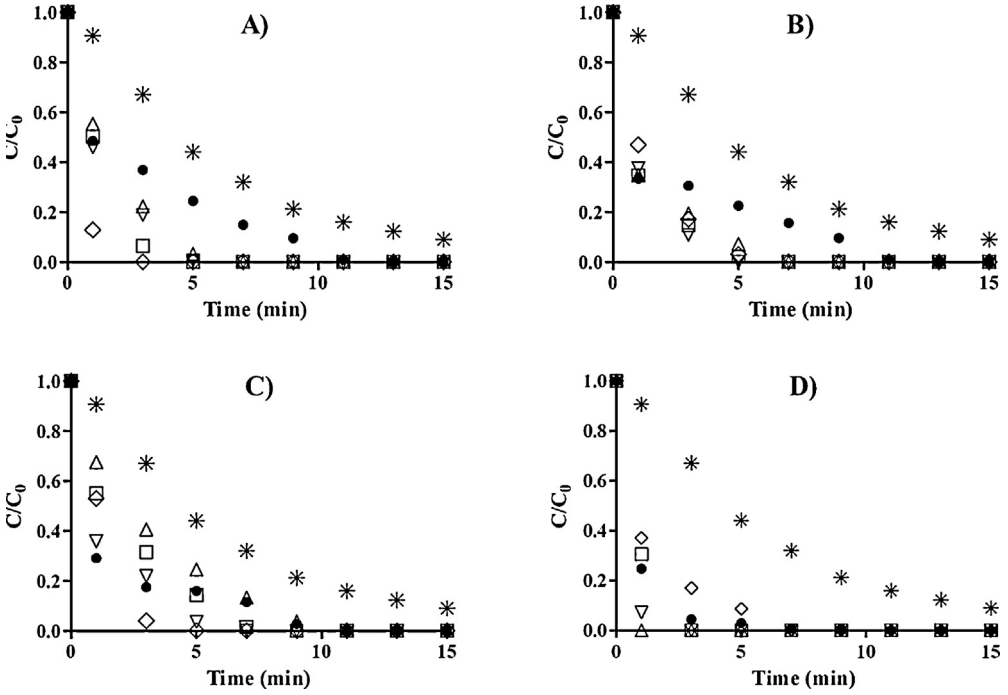

Fig. 6. Time course of DTZ degradation fraction with the UV/AC system. (*), Direct photolysis; (●), UV/AC;(□), UV/CA-H$^{\bullet}$; (△), UV/CA-e_{aq}^{-}; (▽), UV/CA-HO$^{\bullet}$; (◊),UV/CA-0. (A) Carbon C; (B) Carbon M; (C) Carbon S; (D) Carbon W. $[DTZ]_0 = 25\ mg\ L^{-1}$; pH = 6.5; $T = 298$ K.

of the treatment applied (oxidizing or reducing agents), irradiation of the activated carbon increases its synergic activity. The chemical properties of the treated carbons (Table 4S, in supporting information) show that both treatments increase the percentage of —Ph—OH, C—O (ester/anhydride) groups in comparison to the original carbon. In order to confirm that these groups participate in the synergic activity of the activated carbon, the remaining activated carbons studied were treated under the same experimental conditions. Fig. 6 and Table 3 report the percentage DTZ degradation as a function of treatment time in the presence of the treated activated carbons and the percentage synergic contribution for one minute of treatment, respectively.

The results show that, regardless of the activated carbon sample considered, its synergic activity is enhanced by the gamma radiation treatment, although this behavior depends on the baseline material. Thus, the reaction rate varies in the order W—HO$^{\bullet}$ > W—e^{-}_{aq} > W > W—H$^{\bullet}$ > W-0 for carbon W but in the order M—H$^{\bullet}$ > M—e^{-}_{aq} > M—HO$^{\bullet}$ > M-0 > M for carbon M. When the data in Fig. 6 and Table 3 were related to the textural and chemical properties of the activated carbons, no general trend was found among the 20 samples studied. However, in general, the samples that most enhance the synergic activity of the activated carbon are those with a higher percentage of surface oxygen and, among these, those with higher percentages of ester/anhydride groups and of carbon atoms with sp^2 hybridization.

In order to dig deep into the activated carbon characteristics affecting its photocatalytic activity, we have determined the band gap (E_g) of the activated carbons. Thus, based on the DRS, we studied the electronic properties of the materials according to the Kubelka–Munk theory [47–49], which assumes that the radiation falling on a dispersing medium simultaneously undergoes absorption and dispersion, such that the reflected radiation can be defined as a function of the absorption (k) and dispersion (s) constants, as shown in Eq. (19):

$$F(R) = \frac{(1 - R_\infty)}{2R_\infty} = \frac{k}{S} \tag{19}$$

where $F(R)$ is the Kubelka–Munk function corresponding to the absorbance, R_∞ is the reflectance of a sample of infinite thickness with respect to a standard (barium sulfate) for each measured wavelength, k is the absorption coefficient, and S is the dispersion coefficient. If the dispersion of the material is assumed to be constant for the wavelength range measured, Eq. (19) only depends on the absorption coefficient; therefore, the reflectance is the equivalent absorption coefficient, α (Eq. (20)).

$$F(R) = \frac{(1 - R_\infty)^2}{2R_\infty} = \alpha \tag{20}$$

For the different transition mechanisms, the following relationship has been demonstrated between the energy of the incident photons and the band gap energy (E_g) of the material in the absorption process [50,51]:

$$\alpha \cdot h\upsilon = C(h\upsilon - E_g)^n \tag{21}$$

where α is the linear absorption coefficient of the material, h is the Planck constant (4.136×10^{-15} eV s^{-1}), C is the adjustment constant of the model, $h\upsilon$ is the energy of the photon (eV), E_g is the energy of the band gap (eV), and n is the constant for the given type of optical transition, with values of $n = 2$ for indirect allowed transitions, $n = 3$ for indirect forbidden transitions, $n = 1/2$ for direct allowed transitions, and $n = 3/2$ for direct forbidden transitions. Eq. (22) is obtained by substituting Eq. (20) in Eq. (21)

$$(F(R) \cdot h\upsilon)^{1/n} = C(h\upsilon - E_g) \tag{22}$$

Therefore, based on the above equation, it is possible to determine E_g by plotting $(F(R)\cdot h\upsilon)^{1/n}$ against $h\upsilon$.

There is controversy about the value assigned to n and the manner of calculating the band gap, as reported by López et al. in their comparative study [49]. In the present case, we obtained E_g by plotting $(F(R)\cdot h\upsilon)^{1/n}$ against $h\upsilon$ and considering $n = 1/2$ for the direct allowed transitions of the band gap [50,52,53]. Furthermore, we minimized the adjustment error by conducting a double linear adjustment and determining the value of E_g, as the cut-off point of the two lines, as proposed by Chan et al. [54]. As an example,

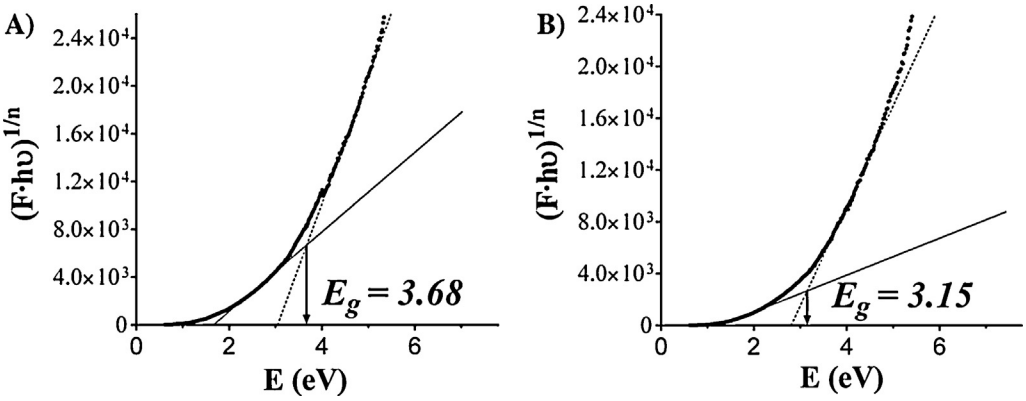

Fig. 7. Calculation of the band gap (E_g) of activated carbons W. A, pristine activated carbon W. B, activated carbon W-e^-_{aq} [54].

Fig. 7 shows the calculation of E_g for activated carbons W and W-e^-_{aq}. Table 4 exhibits the results obtained for all carbon samples studied.

According to the results in Table 4, the activated carbons behave as semiconductor materials and therefore as photoactive materials in the presence of UV radiation, because all E_g values are <4 eV. It can also be observed that the gamma radiation treatment reduces the band gap energy values of the materials and that, in the same series of activated carbons, lower E_g values correspond to higher k_{OB} values (Table 3), especially in series with greater band gap reductions.

The W series show the highest performance in synergic removal (Table 3), although their E_g values are not the lowest among the activated carbons. This may be due to the presence of sulfur heteroatoms in the composition of carbon W, which has higher sulfur concentrations than the other carbons (Table 2S, in supporting information). The presence of sulfur produces an increase in carbon atoms with sp^2 hybridization of the carbons [55,56], which facilitates the transit of electrons, the main triggers of the photocatalytic process that degrades the compound. This is demonstrated by the ratio of carbon atoms with sp^3 and sp^2 hybridization observed in the activated carbons (Table 4S, in supporting information), given that a reduction in this ratio, i.e., a higher percentage of sp^2 hybridization, favors an increase in reaction rates (k_{OB}, Table 3). We found that sp^2 hybridization is increased in the materials modified with gamma radiation, explaining their usually superior behavior in the process under study. Hence, the photocatalytic activity of the carbon is favored not only by the decrease in E_g values but also by the amount of carbon atoms with sp^2 hybridization of the material. Thus, although, in general, the W series has not the lowest E_g values, it obtains the best performance because of its higher fraction of sp^2 hybridization.

Comparison of E_g values with the chemical properties of the activated carbons revealed a clear relationship between E_g and the percentage of surface oxygen. As shown in Fig. 8, in general, all of the carbon series show a decrease in E_g values with an increase in surface oxygen, thereby improving the photoactive activity of the material. There is a minimum E_g value (around 3 eV) below which no further decrease is observed, even when the percentage of surface oxygen increases. This relationship is of major interest in the analysis of carbon as a semiconductor of charged particles, because a reduction in the value of E_g in the carbons means that less energy is required to generate the promotion of electrons. According to these results, the introduction of oxygen atoms into the graphene layers of the activated carbon facilitates the promotion of a greater number of electrons to the conduction band, due to the creation of carbon–oxygen bonds and the formation of new molecular orbitals in the system accompanied by a reduction in the energy between HOMO and LUMO orbitals. Similar results were observed by other authors [57].

These findings indicate the possible mechanism underlying the photoactive activity of the activated carbons. We propose that the photons from UV light would fall on the activated carbons and generate electron–hole pairs through their irradiation with a sufficient amount of energy to promote electrons from the valence band to the conduction band. The photogenerated electrons would spread throughout the graphene layers and reach molecules of the absorbed DTZ and oxygen molecules. The electrons reduce the adsorbed O_2 to form superoxide radicals ($O_2^{\bullet -}$), which can react with the water molecule and trigger the formation of oxidizing radical species [58] that will interact with the compound, contributing to its degradation (Reactions 23–25). Additionally, the presence of adsorbed oxygen avoids recombination of the electron with the

Table 4
Band gap values (E_g) of the activated carbons, calculated according to the Kubelka–Munk method [47,48,54].

Carbón	E_g (eV)	Carbón	E_g (eV)
C	3.65 ± 0.03	S	3.58 ± 0.02
C—H$^\bullet$	3.36 ± 0.02	S—H$^\bullet$	3.63 ± 0.02
C—e^-_{aq}	3.14 ± 0.02	S—e^-_{aq}	3.16 ± 0.02
C—HO$^\bullet$	3.00 ± 0.02	S—HO$^\bullet$	2.92 ± 0.02
C-0	3.04 ± 0.02	S-0	2.98 ± 0.02
M	3.50 ± 0.02	W	3.68 ± 0.02
M—H$^\bullet$	3.13 ± 0.02	W—H$^\bullet$	3.35 ± 0.02
M—e^-_{aq}	3.20 ± 0.02	W—e^-_{aq}	3.15 ± 0.02
M—HO$^\bullet$	3.23 ± 0.02	W—HO$^\bullet$	3.10 ± 0.02
M-0	3.33 ± 0.02	W-0	3.23 ± 0.02

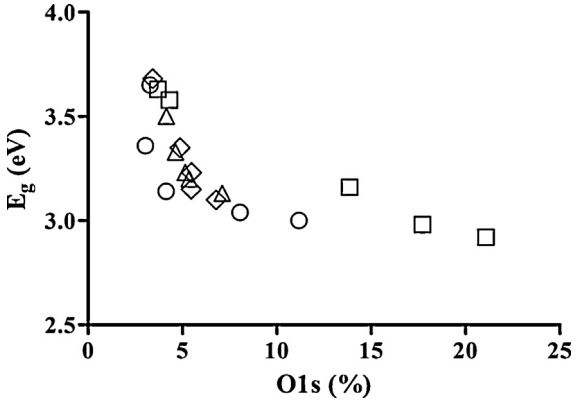

Fig. 8. Relationship between E_g and percentage total surface oxygen of the carbon for the four series of activated carbons. Series C (◯). Series M (△). Series S (□). Series W (◊).

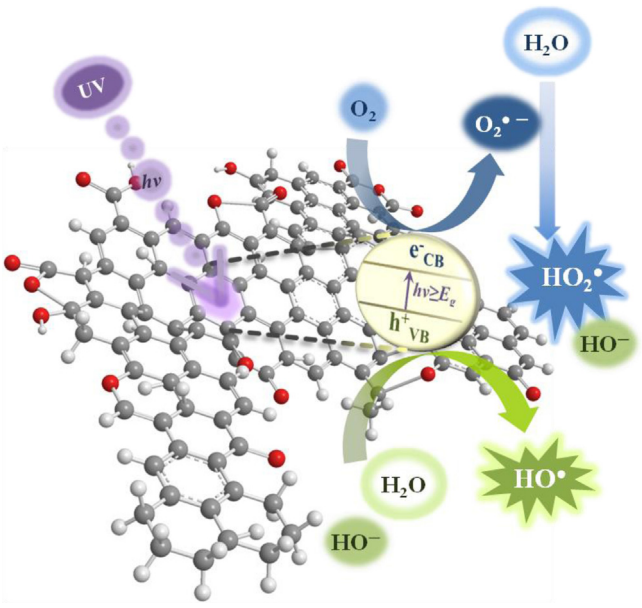

Fig. 9. Action mechanism of activated carbon as photocatalyst in the presence of UV light.

positive hole (Reaction 23), allowing interaction between the water molecule and the free hole and increasing the effectiveness of the photocatalytic process.

$$e_{CB}^{-} + O_2 \rightarrow O_2^{\bullet -} \quad (23)$$

$$O_2^{\bullet -} + H_2O \rightarrow HO_2^{\bullet} + HO^{-} \quad (24)$$

$$2HO_2^{\bullet} \rightarrow O_2 + H_2O_2 \rightarrow O_2 + 2HO^{\bullet} \quad (25)$$

The positive holes are directly responsible for the generation of hydroxyl radicals by interaction with OH^- groups of the carbon surface and by capture of water molecules (Reaction 26). Fig. 9 illustrates the proposed mechanism.

$$h_{VB}^{+} + H_2O \rightarrow HO^{\bullet} + H^{+} \quad (26)$$

3.4. Influence of the presence of dissolved oxygen

Dissolved oxygen has a highly important role in photocatalytic processes [59–61]. Fig. 10 depicts the results obtained by DTZ photodegradation in the presence of activated carbon as catalyst and bubbling nitrogen to avoid the presence of dissolved oxygen.

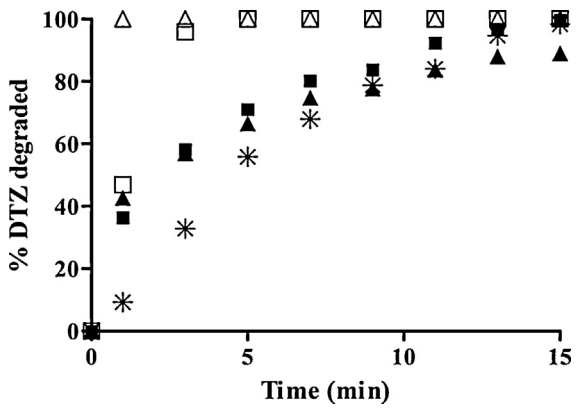

Fig. 10. Influence of dissolved oxygen on DTZ degradation by the UV/AC system. (*), Direct photolysis; (□), UV/S-0 with dissolved oxygen; (■), UV/S-0 without dissolved oxygen; (△), UV/W-e^-_{aq} with dissolved oxygen; (▲), UV/W-e^-_{aq} without dissolved oxygen. $[DTZ]_0 = 25\ mg\ L^{-1}$; pH = 6.5; $T = 298\ K$.

Results show that the presence of dissolved oxygen has a considerable influence on the DTZ removal rate by the UV/AC system, reducing this rate by removing oxygen from the solution. In fact, it can be observed that percentage degradation values obtained in the presence of these activated carbons and in the absence of dissolved oxygen are similar to and approach the values obtained by photolysis. This observation confirms the above-proposed mechanism, given that the absence of dissolved oxygen in the medium produces a lower percentage DTZ degradation because only the positive holes would remain active, transforming the water molecules into hydroxyl radicals, and because the absence of oxygen as electron scavenger reduces the formation of the electron–hole systems. Thus, the consumption of dissolved oxygen with longer treatment time reduces the synergic activity of the activated carbon in the UV/AC system.

3.5. Reutilization of activated carbons in the UV/AC system

Finally, we analyzed a further requirement for activated carbon to act as photocatalyst, i.e., the persistence of its activity over time. For this purpose, we studied the photocatalyst capacity of carbons W, W-e^-_{aq}, S, and S-0 at different DTZ concentrations, recovering and reutilizing them in another photodegradation experiment, analyzing the chemical and textural properties of the UV radiation-treated carbons. We highlight that these reutilized carbons have no adsorption capacity. The results obtained are exhibited in Fig. 11 and Tables 5 and 6, demonstrating that all of

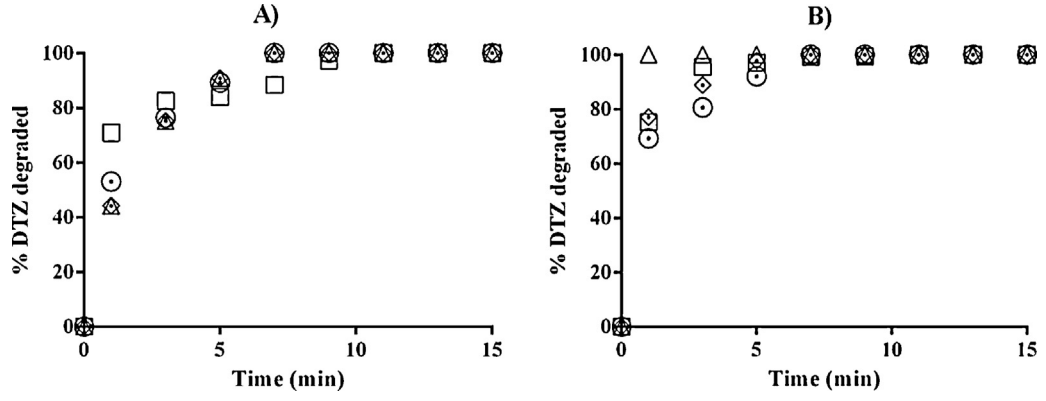

Fig. 11. Reutilization of activated carbons in the process of DTZ removal by UV/AC. (A) Series S: UV/S (□), UV/S reutilized (⊙), UV/S-0 (△), UV/S-0 reutilized (◈); (B) Series W: UV/W (□), UV/W reutilized (◈), UV/W-e^-_{aq} (△), UV/W-e^-_{aq} reutilized (⊙). $[DTZ]_0 = 25\ mg\ L^{-1}$; pH = 6.5; $T = 298\ K$; 5 mg carbon in 30 mL of solution. $\Lambda = 253.70\ nm$.

Table 5
Textural characteristics of the activated carbons irradiated with UV light (λ = 253.70 nm). Exposure time 15 min.

Carbon	S_{BET}[a] ($m^2\ g^{-1}$)	V_T (N_2)[b] ($cm^3\ g^{-1}$)	D_P (N_2)[c] (nm)	S_{Ext}[d] ($m^2\ g^{-1}$)	$V_0(N_2)/V_0(CO_2)$[e]
W	792	0.39	1.96	20.23	1.58
W-0	796	0.40	1.95	20.20	1.54

[a] Surface area determined by N_2 adsorption isotherms at 77 K.
[b] Total pore volume calculated for $p/p_0 = 0.99$.
[c] Mean pore width determined for a cylindrical model from N_2 adsorption isotherm (77 K).
[d] External surface determined by the *t* method.
[e] Relationship between the total volume determined by N_2 (77 K) and by CO_2 (273 K).

Table 6
Oxygenated groups present on the carbon surface after irradiation with UV light. pH = 6.5; *T* = 298 K; Sampling time: 3 and 15 min. λ = 253.70 nm.

Carbon	Sampling time	C=O (quinone) (%)	C=O (ester, carbonyl) (%)	R—OH, C—O—C (%)	Ph—OH, C—O (ester, anhydride) (%)	O1s (%)
W	0	31.95	21.27	24.36	11.15	3.42
W	3	25.83	26.33	25.51	10.61	4.69
W	15	24.87	28.76	21.52	15.39	5.22
W—H$^{\bullet}$	0	32.93	23.68	21.91	11.11	4.87
W—H$^{\bullet}$	3	28.45	24.12	24.04	12.38	4.96
W—H$^{\bullet}$	15	31.85	24.11	18.68	12.39	4.72
W—e_{aq}^-	0	31.24	20.20	21.16	14.77	5.46
W—e_{aq}^-	3	37.14	26.88	17.94	7.85	5.47
W—e_{aq}^-	15	33.13	19.89	22.23	13.96	5.12
W—HO$^{\bullet}$	0	33.18	25.42	10.35	21.93	6.78
W—HO$^{\bullet}$	3	32.42	24.54	18.36	14.90	5.92
W—HO$^{\bullet}$	15	34.38	27.48	15.00	15.22	6.33
W-0	0	31.05	21.50	21.28	14.51	5.48
W-0	3	34.70	24.82	19.16	11.09	5.40
W-0	15	31.78	22.83	23.16	11.12	5.73

the reutilized activated carbons show a similar catalytic activity to that observed for the original carbons (Fig. 11).

We also observed that UV radiation produces no modification in carbon porosity (Table 5). Furthermore, we used XPS to analyze the surface chemistry of the series W carbons after UV radiation exposure for 3 and 15 min. The results in Table 6 indicate that the surface chemistry of the original W activated carbon underwent slight modifications, whereas differences were minimal on the irradiated W activated carbon samples. These results demonstrate that the photocatalytic activity of the activated carbon is maintained over time and that UV radiation does not produce major chemical or textural modifications in it.

4. Conclusions

The results of this study demonstrate that the direct DTZ photodegradation rate is not influenced by the solution pH.

The presence of activated carbon during the DTZ photodegradation process markedly increases the removal rate, regardless of the activated carbon used. The results obtained indicate that activated carbon W exerts the greatest synergic effect on DTZ removal by the UV/AC system, with a synergic contribution >53% at one minute of treatment.

Regardless of the activated carbon sample considered, its synergic activity is, in general, enhanced by the gamma radiation treatment.

The textural and chemical properties of the activated carbons used show no clear relationship with their synergic contribution. However, the synergic activity of the activated carbon is more greatly enhanced by the samples with higher percentages of surface oxygen and, among these, the samples with higher percentages of carbon atoms with sp^2 hybridization.

Determination of the activated carbon band gap demonstrated that these materials behave as semiconductor materials and therefore as photoactive materials in the presence of UV radiation, because all E_g values are <4 eV. In general, the gamma radiation treatment reduces the band gap energy of the materials and, within the same series of activated carbons, lower E_g values correspond to higher k_{OB} values. We indicate that the percentage of carbon atoms with sp^2 hybridization is increased in the gamma radiation-modified materials, explaining their usually superior behavior in DTZ photodegradation.

We highlight that: (i) the photocatalytic activity of reutilized activated carbons is similar to that of the original carbons, (ii) the presence of dissolved oxygen enhances DTZ removal by UV/AC, and (iii) UV radiation produces very slight chemical modifications on the activated carbons.

The W series show the highest performance in synergic removal, although their E_g values are not the lowest among the activated carbons. This may be due to the presence of sulfur heteroatoms in the composition of carbon W, which has higher sulfur concentrations than the other carbons.

Based on these results, an action mechanism for the photocatalytic removal of DTZ in the presence of activated carbon is proposed, in which the activated carbon acts as a photocatalyst, promoting electrons of the valence band to the conduction band and increasing the generation of OH$^{\bullet}$ radicals in the medium.

Acknowledgements

The authors are grateful for the financial support provided by the Junta de Andalucía (RNM7522) and the Spanish Ministry of Science and Innovation (CTQ2011-29035-C02-02).

Appendix A. Supplementary data

Supplementary data associated with this article can be found, in the online version, at http://dx.doi.org/10.1016/j.apcatb.2013.06.003.

References

[1] C.G. Daughton, T.A. Ternes, Environmental Health Perspectives 107 (1999) 907–938.
[2] K. Kümmerer, Journal of Environment Management 90 (2009) 2354–2366.

[3] C. Abegglen, A. Joss, C.S. McArdell, G. Fink, M.P. Schlüsener, T.A. Ternes, H. Siegrist, Water Research 43 (2009) 2036–2046.
[4] O.A.H. Jones, N. Voulvoulis, J.N. Lester, Critical Reviews in Environment Science and Technology 35 (2005) 401–427.
[5] T. Ternes, Preprints of Papers Presented at National Meeting – (American Chemical Society, Division of Environmental Chemistry) 40 (2000) 98–100.
[6] M. Carballa, F. Omil, J.M. Lema, M.a. Llompart, C. Garcıïa-Jares, I. Rodrıïguez, M. Gómez, T. Ternes, Water Research 38 (2004) 2918–2926.
[7] J.E. Drewes, P. Fox, M. Jekel, Journal of Environmental Science and Health. Part A, Toxic/hazardous Substances & Environmental Engineering 36 (2001) 1633–1645.
[8] L.J. Fono, E.P. Kolodziej, D.L. Sedlak, Environmental Science & Technology 40 (2006) 7257–7262.
[9] A. Putschew, S. Wischnack, M. Jekel, Science of the Total Environment 255 (2000) 129–134.
[10] W. Seitz, W.H. Weber, J.Q. Jiang, B.J. Lloyd, M. Maier, D. Maier, W. Schulz, Chemosphere 64 (2006) 1318–1324.
[11] T. Heberer, Toxicology Letters 131 (2002) 5–17.
[12] W. Kalsch, Science of the Total Environment 225 (1999) 143–153.
[13] A. Haiß, K. Kümmerer, Chemosphere 62 (2006) 294–302.
[14] S. Pérez, D. Barceló, Analytical and Bioanalytical Chemistry 387 (2007) 1235–1246.
[15] J. Rivera-Utrilla, M. Sánchez-Polo, Applied Catalysis B 39 (2002) 319–329.
[16] M. Sánchez-Polo, J. Rivera-Utrilla, Carbon 41 (2003) 303–307.
[17] T.A. Ternes, J. Stüber, N. Herrmann, D. McDowell, A. Ried, M. Kampmann, B. Teiser, Water Research 37 (2003) 1976–1982.
[18] F.J. Real, F. Javier Benitez, J.L. Acero, J.J.P. Sagasti, F. Casas, Industrial and Engineering Chemistry Research 48 (2009) 3380–3388.
[19] J.H. Carey, J. Lawrence, H.M. Tosine, Bulletin of Environment Contamination and Toxicology 16 (1976) 697–701.
[20] S. Ahmed, M.G. Rasul, R. Brown, M.A. Hashib, Journal of Environment Management 92 (2011) 311–330.
[21] C.A. Leon, L.R. Radovic, Chemistry and Physics of Carbon 24 (1994) 213–310.
[22] A.Y. Shan, T.I.M. Ghazi, S.A. Rashid, Applied Catalysis A 389 (2010) 1–8.
[23] C.M. Teh, A.R. Mohamed, Journal of Alloys and Compounds 509 (2011) 1648–1660.
[24] T.T. Lim, P.S. Yap, M. Srinivasan, A.G. Fane, Critical Reviews in Environment Science and Technology 41 (2011) 1173–1230.
[25] H. Choi, E. Stathatos, D.D. Dionysiou, Applied Catalysis B 63 (2006) 60–67.
[26] G. Li Puma, A. Bono, D. Krishnaiah, J.G. Collin, Journal of Hazardous Materials 157 (2008) 209–219.
[27] T. Cordero, C. Duchamp, J.M. Chovelon, C. Ferronato, J. Matos, Journal of Photochemistry and Photobiology A 191 (2007) 122–131.
[28] J. Matos, A. Garcia, T. Cordero, J.M. Chovelon, C. Ferronato, Catalysis Letters 130 (2009) 568–574.
[29] M.H. Baek, W.C. Jung, J.W. Yoon, J.S. Hong, Y.S. Lee, J.K. Suh, Journal of Industrial and Engineering Chemistry 19 (2013) 469–477.
[30] J. Rivera-Utrilla, M. Sánchez-Polo, M.M. Abdel Daiem, R. Ocampo-Pérez, Applied Catalysis B 126 (2012) 100–107.
[31] J.L. Figueiredo, M.F.R. Pereira, Catalysis Today 150 (2010) 2–7.
[32] F. Rodríguez-reinoso, Carbon 36 (1998) 159–175.
[33] W. Wang, C.G. Silva, J.L. Faria, Applied Catalysis B 70 (2007) 470–478.
[34] M. Haro, L.F. Velasco, C.O. Ania, Catalysis Science & Technology 2 (2012) 2264–2272.
[35] L.F. Velasco, I.M. Fonseca, J.B. Parra, J.C. Lima, C.O. Ania, Carbon 50 (2012) 249–258.
[36] L.F. Velasco, V. Maurino, E. Laurenti, I.M. Fonseca, J.C. Lima, C.O. Ania, Applied Catalysis A 452 (2013) 1–8.
[37] S.P. Mezyk, D.M. Bartels, Journal of Physical Chemistry A 101 (1997) 6233–6237.
[38] P.M. Alvárez, J.F. García-Araya, F.J. Beltrán, I. Giráldez, J. Jaramillo, V. Gómez-Serrano, Carbon 44 (2006) 3102–3112.
[39] J. Rivera-Utrilla, M. Sánchez-Polo, Langmuir 20 (2004) 9217–9222.
[40] M. Sánchez-Polo, U. Von Gunten, J. Rivera-Utrilla, Water Research 39 (2005) 3189–3198.
[41] E. Atinault, V. De Waele, U. Schmidhammer, M. Fattahi, M. Mostafavi, Chemical Physics Letters 460 (2008) 461–465.
[42] G.V. Buxton, C.L. Greenstock, W.P. Helman, A.B. Ross, Journal of Physical and Chemical Reference Data 17 (1988) 2593–2600.
[43] B.G. Ershov, M. Kelm, A.V. Gordeevb, E. Janata, Physical Chemistry Chemical Physics 4 (2002) 1872–1875.
[44] J.A. LaVerne, M.R. Ryan, T. Mu, Radiation Physics and Chemistry 78 (2009) 1148–1152.
[45] O. Roth, J.A. Laverne, Journal of Physical Chemistry A 115 (2011) 700–708.
[46] M. Sánchez-Polo, J. Rivera-Utrilla, Applied Catalysis B 67 (2006) 113–120.
[47] P. Kubelka, Journal of the Optical Society of America 38 (1948) 448–457.
[48] P. Kubelka, F. Munk, Zeitschrift für Technische Physikalische (Leipzig) 12 (1931) 593–601.
[49] R. López, R. Gómez, Journal of Sol-Gel Science and Technology 61 (2012) 1–7.
[50] S. Adhikari, H.R. Aryal, D.C. Ghimire, G. Kalita, M. Umeno, Diamond and Related Materials 17 (2008) 1666–1668.
[51] L. Escobar-Alarcón, A. Arrieta, E. Camps, S. Muhl, S. Rodil, E. Vigueras-Santiago, Applied Surface Science 254 (2007) 412–415.
[52] N. Ahmad, N.A. Tahir, M. Rusop, in: L. Yuan (Ed.), Amorphous Carbon Thin Films Deposited by Thermal CVD Using Camphoric Carbon as Precursor, 2012, pp. 646–650.
[53] T.S. Chen, S.E. Chiou, S.T. Shiue, Thin Solid Films 528 (2013) 86–92.
[54] G.H. Chan, B. Deng, M. Bertoni, J.R. Ireland, M.C. Hersam, T.O. Mason, R.P. Van Duyne, J.A. Ibers, Inorganic Chemistry 45 (2006) 8264–8272.
[55] L. Kumari, V. Prasad, S.V. Subramanyam, Carbon 41 (2003) 1841–1846.
[56] L. Kumari, S.V. Subramanyam, Applied Physics A: Materials Science and Processing 95 (2009) 343–349.
[57] H. Tamon, M. Okazaki, Journal of Colloid and Interface Science 179 (1996) 181–187.
[58] H.P. Boehm, Carbon 50 (2012) 3154–3157.
[59] X. Van Doorslaer, P.M. Heynderickx, K. Demeestere, K. Debevere, H. Van Langenhove, J. Dewulf, Applied Catalysis B 111/112 (2012) 150–156.
[60] N.P. Xekoukoulotakis, C. Drosou, C. Brebou, E. Chatzisymeon, E. Hapeshi, D. Fatta-Kassinos, D. Mantzavinos, Catalysis Today 161 (2011) 163–168.
[61] T.A. McMurray, P.S.M. Dunlop, J.A. Byrne, Journal of Photochemistry and Photobiology A 182 (2006) 43–51.